Analysis of charge transfer and recombination for the poly(3-hexylthiophene):[6,6]-phenyl C61 butyric acid methyl ester organic solar cells with iron oxide nanoparticles in various layers

Eung-Kyu Park, Ji-Hwan Kim, Hyeong Jun Cho, Dong-Hoon Lee, and Yong-Sang Kim

Citation: Applied Physics Letters **107**, 153903 (2015); doi: 10.1063/1.4933270
View online: http://dx.doi.org/10.1063/1.4933270
View Table of Contents: http://scitation.aip.org/content/aip/journal/apl/107/15?ver=pdfcov
Published by the AIP Publishing

Analysis of charge transfer and recombination for the poly(3-hexylthiophene):[6,6]-phenyl C_{61} butyric acid methyl ester organic solar cells with iron oxide nanoparticles in various layers

Eung-Kyu Park, Ji-Hwan Kim, Hyeong Jun Cho, Dong-Hoon Lee, and Yong-Sang Kim[a)]
School of Electronic and Electrical Engineering, Sungkyunkwan University, Suwon, Gyeonggi 16419, South Korea

(Received 7 April 2015; accepted 4 October 2015; published online 14 October 2015)

An improved organic solar cell's performance was obtained by focusing on the effects of iron oxide (Fe_2O_3) nanoparticles (NPs) within the different layers of P3HT:PCBM solar cells. We investigated the recombination mechanism in organic solar cells using the current density-voltage (J-V) characteristics at various light intensities and also analyzed the electrochemical impedance. Shockley–Read–Hall (SRH) recombination, which is dependent on the trap states, surface roughness, resistance and charge transport, controls the cell efficiency. The device performance was compared by adding iron oxide nanoparticles in the active layer and Poly(3,4-ethylenedioxythiophene):poly(styrenesulfonate) (PEDOT:PSS) layer, respectively. Also the iron oxide nanoparticle layer was inserted as an interface layer between active and PEDOT:PSS layers. The solar cell without NPs showed a 2.68% power conversion efficiency while that with Fe_2O_3 NPs as an interface layer showed a higher power conversion efficiency of 3.83% under air mass (AM) 1.5G illumination. The device with NPs as an interface layer showed a smooth surface roughness (1.16 nm), lower charge recombination (1.06(kT/e)), and lower parasitic resistance (254 Ω cm^2). © *2015 AIP Publishing LLC*. [http://dx.doi.org/10.1063/1.4933270]

The organic solar cells (OSCs) are attracting a great deal of attention as a renewable energy source owing to their advantages of easy fabrication, low-cost, light weight, and the possibility to fabricate flexible devices. Recent studies have reported remarkably improved power conversion efficiency (PCE) of the OSCs up to 5% for poly(3-hexylthiophene):[6,6]-phenyl C_{61} butyric acid methyl ester (P3HT:PCBM) cells.[1] However, in the polymer and fullerene blend, the PCE of the devices are limited as the charge carrier mobility is comparatively low, with a short exciton diffusion length in the active layer.[2] In order to improve the performance of the OSCs, it is required to introduce other additive materials.

The addition of light scattering materials revamps the light intensity in the device, resulting in an increased light absorption. An efficient light trapping material in the active layer will enhance the photon absorption without the need for a thick film. Recently, the use of surface plasmon resonance (SPR) effect, due to the scattering of light and/or with the increase of path length of the absorbed light, has attracted much attention as a means for increasing the photocurrents of OSCs.[3–9] As proposed by Paci *et al.*, the use of metallic nanoparticle (NP) has a dual advantage on the efficiency of OSCs.[10] Along with the increase of path length of the absorbed light, NPs also enhance the structural stability of the layer leading to a slower device degradation rate during prolonged illumination. In order to improve the efficiency of organic solar cells, the approach addressed in this paper is the careful use of metal oxide nanoparticle's properties to induce surface plasmons which enhances the optical absorption and photocurrent generation over a broad range of visible wavelengths.[11] In our previous work, we confirmed the role of Fe_2O_3 NPs in the enhancement of the cell performance. A 2.79% PCE was obtained when the metal oxide NPs was mixed in the PEDOT:PSS layer with fluorine doped tin oxide (FTO) as the substrate and TiO_2 as the hole blocking layer.[12]

In this study, we improved and compared the photovoltaic performance of organic solar cell by introducing iron oxide NPs into the different layer. We compared the performance of OSCs by adding the commercially available Fe_2O_3 NPs (Sigma Aldrich, Korea) in the buffer layer and active layer and also used it as an artificial buffer layer. Transmission electron microscopy confirmed the size of NPs to be ~50 nm (supplementary material, Fig. S1).[22] Fe_2O_3 NPs in 1 wt. % concentration were used for the optimal condition. Usually, a higher concentration of Fe_2O_3 (>1 wt. %) results in the blockage of hole transfer and decreases current density (supplementary material, Fig. S2).[22] The device structures (Figure 1) are as followings: (a) ITO/ZnO/P3HT:PCBM: (Fe_2O_3)/PEDOT:PSS/Ag, (b) ITO/ZnO/P3HT:PCBM/ Fe_2O_3/PEDOT:PSS/Ag, and (c) ITO/ZnO/P3HT:PCBM/PEDOT: PSS:(Fe_2O_3)/Ag. ZnO was used as a buffer layer for hole-blocking between the active layer and bottom electrode. ZnO solution was spin coated onto indium tin oxide (ITO) substrate and then annealed at 200 °C for 20 min in ambient air condition. In case of NPs mixed active layer (Fig. 1(a)), a mixture of 1 wt. % Fe_2O_3 NPs and P3HT:PCBM was deposited on the ZnO layer by spin coating. Whereas, in case of the other devices (Figs. 1(b) and 1(c)), only the P3HT:PCBM was spin coated on the ZnO layer. Addition of NPs in the active layer marginally increased the surface roughness but was uniformly distributed, and can be seen in surface morphology and phase images in Fig. S3 (supplementary material).[22] The mixture of P3HT:PCBM (P3HT:PCBM = 1:1 weight ratio) was dissolved

a)Author to whom correspondence should be addressed. Electronic mail: yongsang@skku.edu. Tel.: +82-31-299-4323.

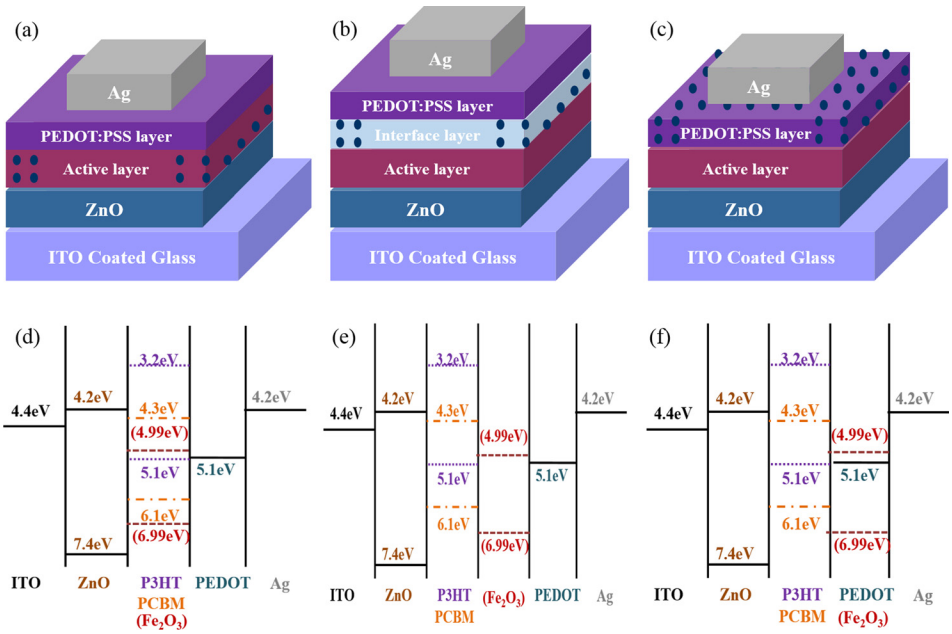

FIG. 1. The schematic of inverted organic solar cell with iron oxide NPs in three different layers ((a)–(c)), Energy band diagram of devices ((d)–(f)).

in chlorobenzene (40 mg/ml). The thickness of active layer was 100 nm in this case. In order to deposit PEDOT:PSS solution, hexamethyldisilazane (HMDS) was first spin coated on the active layer. Thermal pre-annealing was conducted at 160 °C for 10 min in a dry oven in ambient air. Ag top electrode (100 nm) was deposited on PEDOT:PSS layer by thermal evaporation by defining an active area of 0.1 cm^2. Figures 1(d)–1(f) show the energy band diagram of different device structures.[13] Entire fabrication and measurement processes were conducted in ambient air.

The electrical properties of all devices with iron oxide NPs in different layer were characterized by means of electrochemical impedance spectroscopy (EIS), which is a powerful technique widely used to study the interface charge transport process. The measurement was performed in the dark, with electrical frequencies ranging from 100 Hz to 1 MHz.

Figures 2(a) and 2(b) show the frequency-dependent real and imaginary parts of the impedance of the devices with NPs in different layer. Figure 2(a) indicates that real part of the impedance is attributed by two types of resistance, namely, low frequency (<100 Hz) and high frequency (>5000 Hz), respectively. R_s (High frequency) represents the ohmic resistance, including the electrodes and bulk resistance in the active layer. R_p (Low frequency) is associated with the interface charge transport process, defined by the charge transfer resistance. The coarse morphology of the blended film consequence in poor contact between the hole transport layer and cathode and increases the resistance. Also, the change in surface morphology eventuates in a deteriorated device efficiency. The value of R_p of the cell with interface NP layer is 254 Ω cm^2, the smallest of all devices. The small R_p provides more efficient charge transport. As we all know, this charge transfer process has a certain speed reflected in faradaic current which is dependent on surface roughness of the electrodes (supplementary material, Fig. S4).[22] The interface NPs layered device shows the smallest roughness (1.16 nm). It is obvious that the electron transfer in a smoother interface is faster than in a highly roughed device. The constant phase element (CPE) is often used in place of a capacitance-like element to compensate for inhomogeneity in the interface, such as porosities, roughness, and surface states with $\mathrm{CPE} = \frac{1}{(CPE-T)(j\omega)^{(CPE-P)}}$. CPE is defined by two values, CPE-T and CPE-P. If CPE-P equals 1, then the CPE is identical to an ideal capacitor without defects and/or grain boundary.[14,15] The value of CPE-T and CPE-P of the cell with interface NPs layer is 0.13 $\mu F/cm^2$

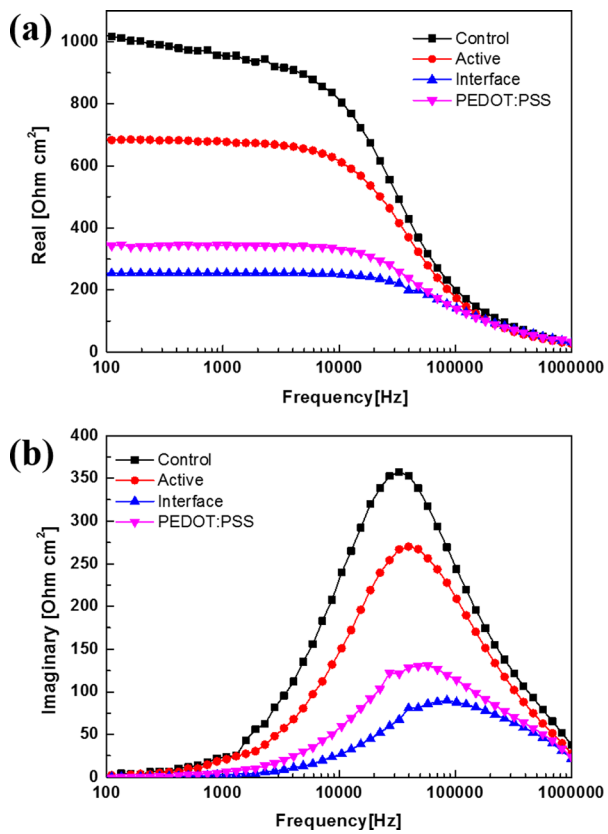

FIG. 2. (a) The frequency-dependent real parts (b) the frequency-dependent imaginary parts in the impedance spectra of the devices with iron oxide NPs in three different layers.

and 0.95, respectively. Thus, the capacitance of the device with interface layer is best close to an ideal capacitor. The parameters determined after the fitting of experimental data are summarized in Table I (supplementary information Fig. S5).[22]

Figure 2(b) shows the frequency-dependent imaginary part of the impedance of different devices. This plot is usually used to evaluate the relaxation frequency of most resistive contribution. It can be seen that the characteristic frequency ($f_{\max}$) centered at peak shifted to high frequency with the interface Fe_2O_3 NPs layered device. The $f_{\max}$ is related to the characteristic relaxation time (τ). The values can be defined by the relation: $f_{max} \propto 1/\tau$. The value of $f_{\max}$ of the device with interface Fe_2O_3 NPs layer is highest in all devices (84.78 kHz). Thus, the value of τ of the device with iron oxide NPs in interface is the smallest of all devices. However, the relaxation process is related to a possible release of space charge. The small τ suggests efficient dissociation of exciton at the interface between P3HT and PCBM and charge transport in the active layer.

Figure 3(a) shows the semi log plot of dependence of open circuit voltage on the light intensity. The charge recombination studies at V_{oc} can provide detailed information of various mechanisms. The relationship between light intensity and V_{oc} is given by[16–18]

$$\delta V_{OC} = \frac{kT}{e}\ln(I) + const, \quad (1)$$

where k is the Boltzmann constant, T is the temperature, e is the electronic charge, and I is the incident light intensity. When the additional mechanism of SRH trap-assisted recombination is involved, a stronger dependence of V_{oc} on light intensity with a slope greater than kT/e is observed.[16] The higher value of the slope coefficient is associated with the strength of trap-assisted recombination. The control device showing a slope of 1.15(kT/e) is indicative of trap-assisted recombination. For active, interface, and PEDOT:PSS layers, the slope values are 1.54(kT/e), 1.06(kT/e), and 3.95(kT/e), respectively. This implies that the interface iron oxide reduced the density of traps between the active layer and Ag contact, and hence SRH recombination is suppressed. The SRH recombination due to trap states can be clearly observed at low light intensities, where the cell efficiency becomes highly dependent on the bias and light intensity (supplementary material, Fig. S6).[22]

The J_{sc} can be correlated to light intensity (I) by[18]

$$J_{SC} \propto I^{\alpha} (\alpha \leq 1). \quad (2)$$

At short circuit, the bimolecular recombination should be minimum ($\alpha ab \approx 1$) for maximum carrier sweep out. Any deviation from $\alpha \approx 1$ implies bimolecular recombination. Figure 3(b) shows the log-log scale relationships of J_{sc} as a function of light intensity, calculated using the power law described above.[19] The fitting of the data yielded $\alpha = 0.931$ for the control device, which can be attributed to the bimolecular recombination. For active, interface, and PEDOT:PSS layers, the α values are 0.917, 0.966, and 0.905, respectively.

TABLE I. EIS measurement of organic solar cells with iron oxide NPs in three different layers.

	R_s (Ω cm^2)	R_p (Ω cm^2)	CPE-T (μF/cm^2)	CPE-P	f_{max} (kHz)
Control	30.9	1017	0.18	0.93	27.10
Active	36.7	675	0.32	0.94	27.10
Interface	30.4	254	0.13	0.95	84.70
PEDOT:PSS	33.5	351	0.16	0.92	58.00

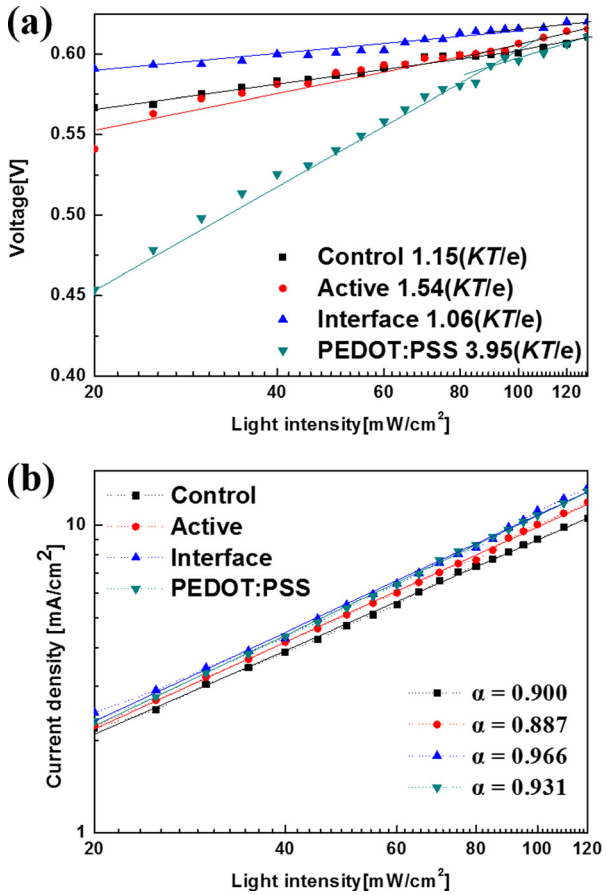

FIG. 3. (a) The measured V_{oc} of organic solar cells with iron oxide NPs in three different layers as a function of illumination intensity (symbols), together with linear fits of the data (solid lines). (b) Measured J_{sc} of organic solar cells with iron oxide NPs in three different layers plotted against light intensity (symbols) on the logarithmic scale and fitted yield α (dotted line).

The measured J-V characteristics under AM 1.5G (100 mW/cm^2) irradiation intensity of organic solar cells with and without iron oxide NPs (three different architecture) are shown in Figure 4(a). The control device showed a short circuit density (J_{sc}) of 9.01 mA/cm^2. The addition of NPs in active layer increased the J_{sc} to 10.31 mA/cm^2. The device with NPs as an interface layer gave a J_{sc} of 11.13 mA/cm^2 while the device with NPs in PEDOT:PSS showed a comparatively lower J_{sc} of 10.77 mA/cm^2. The performance of all the organic solar cells is summarized in Table II.

Figure 4(b) shows the measured external quantum efficiency (EQE) (K3100, McScience) of OSCs. Incident photon conversion efficiency analysis of all the OSCs was also performed and is shown in Fig. S7 (supplementary material).[22] The spectral range of IPCE and EQE enhancement and the presence of peak at ~600 nm can be attributed to a phenomenon of LSPR formation and increase in scattering of light due to the use of NPs (supplementary material, Fig. S8).[22]

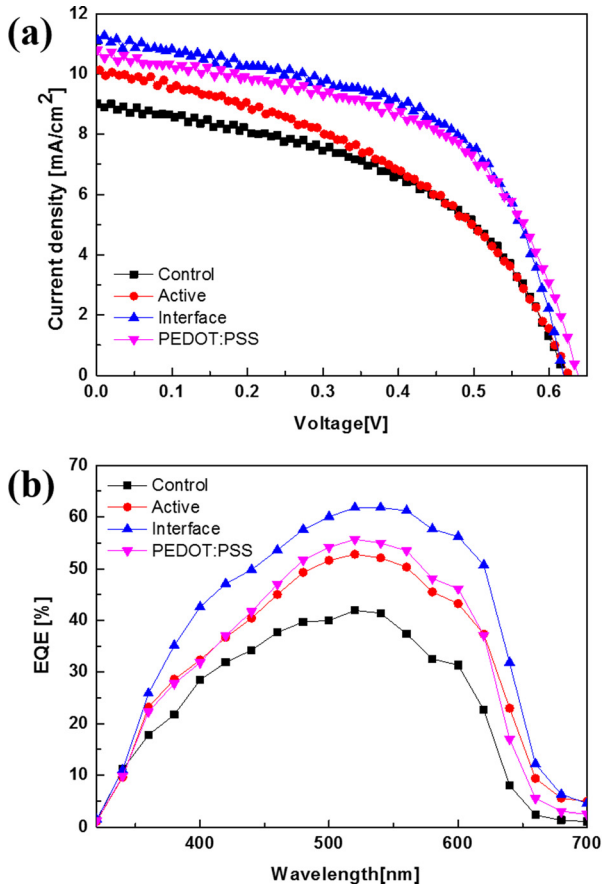

FIG. 4. Inverted solar cells with iron oxide NPs in three different layers. (a) J-V characteristics under AM 1.5G irradiation at 100 mW/cm^2. (b) External quantum efficiency.

TABLE II. J-V characteristic of organic solar cells with iron oxide NPs in three different layers.

	J_{sc} (mA/cm^2)	V_{oc} (V)	F.F	PCE (%)
Control	9.01	0.61	0.48	2.68
Active	10.31	0.61	0.48	3.01
Interface	11.13	0.61	0.55	3.83
PEDOT:PSS	10.77	0.62	0.53	3.68

The light scattering lengthened the optical path in the active layer, thereby trapping it inside.[19–21] A 40% increase in EQE was obtained due to the additional interface layer of NPs. The improvement of J_{sc} shown in Figure 4(a) can be verified from the EQE results.

In summary, we investigated the effect of iron oxide NPs in different layers for light harvesting in organic solar cells. The solar cells with iron oxide NPs blended interface layer showed a high performance of 3.83% under AM 1.5G illumination. The device had a lower charge transfer resistance of 254 Ω cm^2, SRH trap-assisted recombination monomolecular slope of 1.06 (kT/e), and 0.966 bimolecular recombination. A 40% increase in power conversion efficiency was obtained between the control device and optimized device due to the addition of iron oxide NPs.

This work was supported under the framework of international cooperation program managed by National Research Foundation of Korea (No. 2014K2A2A2000803) and also supported by the Human Resources Development program (No. 20144030200580) of the Korea Institute of Energy Technology Evaluation and Planning (KETEP) grant funded by the Korea Government Ministry of Trade, Industry and Energy.

[1]K. Kim, J. Liu, M. A. G. Namboothiry, and D. L. Carroll, Appl. Phys. Lett. **90**, 163511 (2007).
[2]K. M. Coakley and M. D. McGehee, Chem. Mater. **16**, 4533 (2004).
[3]M. G. Kang, T. Xu, H. J. Park, H. X. Luo, and L. J. Guo, Adv. Mater. **22**, 4378 (2010).
[4]K. Tvingstedt, V. Andersson, F. Zhang, and O. Inganäs, Appl. Phys. Lett. **91**, 123514 (2007).
[5]F. C. Chen, J. L. Wu, C. L. Lee, Y. Hong, C. H. Kuo, and M. H. Huang, Appl. Phys. Lett. **95**, 013305 (2009).
[6]A. J. Morfa, K. L. Rowlen, T. H. Reilly, M. J. Romero, and J. V. D. Lagemaat, Appl. Phys. Lett. **92**, 013504 (2008).
[7]A. P. Kulkarni, K. M. Noone, K. Munechika, S. R. Guyer, and D. S. Ginger, Nano Lett. **10**, 1501 (2010).
[8]W. C. H. Choy, Chem. Commun. **50**, 11984 (2014).
[9]X. Li, W. C. H. Choy, H. Lu, W. E. I. Sha, and A. H. P. Ho, Adv. Funct. Mater. **23**, 2728 (2013).
[10]B. Paci, G. D. Spyropoulos, A. Generosi, D. Bailo, V. R. Albertini, E. Startakis, and E. Kymakis, Adv. Funct. Mater. **21**, 3573 (2011).
[11]C. Groves and N. C. Greenham, Phys. Rev. B **78**, 155205 (2008).
[12]E. K. Park, M. Choi, J. H. Jeun, K. T. Lim, J. M. Kim, and Y. S. Kim, Microelectron. Eng. **111**, 166 (2013).
[13]H. Zhang, Z. Ji, T. Xia, H. Meng, C. Low-kam, R. Liu, S. Pokhrel, S. Lin, X. Wang, Y. P. Liao, M. Wang, L. Li, R. Rallo, R. Damoiseaux, D. Telesca, L. Madler, Y. Cohen, J. I. Zink, and A. E. Nel, ACS Nano **6**(5), 4349 (2012).
[14]Y. Zhang, L. Li, S. Yuan, G. Li, and W. Zhang, Electrochim. Acta **109**, 221 (2013).
[15]G. Perrier, R. D. Bettignies, S. Berson, N. Lemaitre, and S. Guillerez, Sol. Energy Mater. Sol. Cells. **101**, 210 (2012).
[16]S. R. Cowan, A. Roy, and A. J. Heeger, Phys. Rev. B **82**, 245207 (2010).
[17]L. J. A. Koster, V. D. Mihailetchi, R. Ramaker, and P. W. M. Blom, Appl. Phys. Lett. **86**, 123509 (2005).
[18]V. Gupta, A. K. K. Kyaw, D. H. Wang, S. Chand, G. C. Bazan, and A. J. Heeger, Sci. Rep. **3**, 1965 (2013).
[19]F. Monestier, J. J. Simon, P. Torchio, L. Escoubas, F. Florya, S. Bailly, R. D. Bettignies, S. Guillerez, and C. Defranoux, Sol. Energy Mater. Sol. Cells. **91**, 405 (2007).
[20]S. A. Maier and H. A. Atwater, J. Appl. Phys. **98**, 011101 (2005).
[21]B. P. Rand, P. Peumans, and S. R. Forrest, J. Appl. Phys. **96**, 7519 (2004).
[22]See supplementary material at http://dx.doi.org/10.1063/1.4933270 for solar cell electrical and optical characterization.